Journal of Magnetic Resonance 202 (2010) 250–258

Contents lists available at ScienceDirect

Journal of Magnetic Resonance

journal homepage: www.elsevier.com/locate/jmr

SEnD NMR: Sensitivity Enhanced *n*-Dimensional NMR

John M. Gledhill Jr., A. Joshua Wand *

Johnson Research Foundation and Department of Biochemistry & Biophysics, University of Pennsylvania, Philadelphia, PA 19104-6059, USA

ARTICLE INFO

Article history:
Received 21 April 2009
Revised 6 November 2009
Available online 18 November 2009

Keywords:
Radial sampling
Multidimensional Fourier transform
Sensitivity enhanced

ABSTRACT

Sparse sampling offers tremendous potential for overcoming the time limitations imposed by traditional Cartesian sampling of indirectly detected dimensions of multidimensional NMR data. However, in many instances sensitivity rather than time remains of foremost importance when collecting data on protein samples. Here we explore how to optimize the collection of radial sampled multidimensional NMR data to achieve maximal signal-to-noise. A method is presented that exploits a rigorous definition of the minimal set of radial sampling angles required to resolve all peaks of interest in combination with a fundamental statistical property of radial sampled data. The approach appears general and can achieve a substantial sensitivity advantage over Cartesian sampling for the same total data acquisition time. Termed Sensitivity Enhanced *n*-Dimensional or SEnD NMR, the method involves three basic steps. First, data collection is optimized using routines to determine a minimal set of radial sampling angles required to resolve frequencies in the radially sampled chemical shift evolution dimensions. Second, appropriate combinations of experimental parameters (transients and increments) are defined by simple statistical considerations in order to optimize signal-to-noise in single angle frequency domain spectra. Finally, the data is processed with a direct multidimensional Fourier transform and a statistical artifact and noise removal step is employed.

1. Introduction

Introduction of the direct multidimensional Fourier transform [1–3] has allowed for the presentation of various sparse sampling schemes [4–8]. The primary focus of this and related developments has been from the perspective of increasing the speed and resolution of an experiment, with the assumption that sensitivity is not limiting. Because the Fourier transform of non-uniformly sampled data always gives rise to artifacts as a result of the sampling scheme employed, the main goal of developing new sampling schemes is to avoid or reduce artifacts. This is accomplished, for example, by specifically weighting the sampled points [8], by constructing the sampling to shift the artifacts away from a peak or to distribute the artifacts equally though the spectrum so they appear as baseline noise [5,6]. This is made possible by the fact that the artifacts are a function of the sampling scheme. This approach has proven successful in multiple cases [5,9]. Additionally, multiple post acquisition methods have been described to remove artifacts from the spectrum by iteratively analyzing and subtracting the artifact intensity [5,9].

Here the alternative situation is considered, where the goal is to increase the sensitivity of a given spectrum. Briefly, to accomplish this we will use a combination of radial sampling [10] and a previously unexploited statistical property of the data. Recently, we have shown that the defined pattern of artifacts arising from the multidimensional FT of radial sampled data allows the definition of a set of algorithms to optimize angle selection [11,12]. As we demonstrate here, optimized angle set collection for radial sampling provides significant freedom for the further optimization of multidimensional NMR spectra with respect to signal-to-noise (S/N). We will first present the theory and the resulting criteria that suggest how data optimized for S/N should be collected. We then illustrate how an inherent feature of radial sampling provides the subsequent opportunity to utilize non-linear statistical methods to exponentially reduce the noise without introduction of artifact. Providing that the criteria underlying the basic approach are met, a substantial sensitivity advantage can be achieved. In addition, the SEnD approach allows one to assess the appropriateness of a utilizing radial sampling successfully for a given experiment.

2. Theory

The SEnD criteria are developed here. To develop the method we decompose the signal and noise terms into the terms dependent on transients, increments and the lower value comparison. This enables a direct comparison of a Cartesian sampled data set

* Corresponding author. Address: Department of Biochemistry & Biophysics, University of Pennsylvania, 905 Stellar-Chance Laboratories, 422 Curie Blvd., Philadelphia, PA 19104-6059, USA. Fax: +1 215 573 7290.
E-mail address: wand@mail.med.upenn.edu (A.J. Wand).

1090-7807/$ - see front matter © 2009 Elsevier Inc. All rights reserved.
doi:10.1016/j.jmr.2009.11.005

to the equivalent experiment collected with radial sampling and processed with the lower value comparison.

Radial sampling is achieved by linking two or more of the indirect dimensions and linearly sampling a vector at an angle (α) with respect to the two orthogonal time domains [10]. In the case of a three-dimensional experiment, this is achieved by collecting the directly detected time domain signal normally and linking the indirect dimensions by defining $t_1 = \tau\cos(\alpha)$ and $t_2 = \tau\sin(\alpha)$ and linearly sampling the time period τ. The directly acquired dimension is sampled and processed traditionally and therefore will be excluded from this analysis. As a result, Cartesian sampled data is represented as a two-dimensional signal with four quadrature components per increment and radial sampled data is represented as a one-dimensional signal also with four quadrature components per increment.

First, we will analyze the noise terms with respect to the sensitivity parameters. For a typical NMR experiment the noise can often be described with a normal distribution of probability centered upon zero:

$$p(x) = \frac{1}{\sigma\sqrt{2\pi}} e^{-\frac{x^2}{2\sigma^2}} \tag{1}$$

where σ is the standard deviation and x is the amplitude of the noise. The standard deviation of the noise changes as a function of both increments and transients. First, we will analyze how changing the number of increments affects the standard deviation of the noise.

The noise is directly dependent upon the number of increments collected. By definition the Fourier transform is a summation. Thus the noise in each data point is present in summation in the final spectrum. The standard deviation of the noise increases as a function of the square root of the number of increments used. The final standard deviation of the noise, in the case of n transients, may be expressed using the variance sum law [13] and is written as follows:

$$\sigma_{ni} = \sqrt{q(\sigma_1^2 + \sigma_2^2 + \cdots + \sigma_n^2)} \tag{2}$$

where σ_n is the standard deviation of the noise for the nth increment, σ_{ni} is the standard deviation of the noise after collecting n increments and q is the number of quadrature components. The number of quadrature components is constant for all cases that we use to develop the SEnD criteria and therefore will be dropped from subsequent expressions.

If acquisition parameters are kept constant while the number of increments is varied such that the standard deviation of the noise of each increment is constant, the final standard deviation of the noise is a function of the square root of the number of increments:

$$\sigma_{ni} = \sigma_s\sqrt{n} \tag{3}$$

Here the individual noise standard deviations for the n components has been replaced with a common value σ_s.

If apodization is applied to the data then the standard deviation of the noise is scaled for each increment and the equation relating the number of points to the final standard deviation must be rewritten to include the apodization term, i.e.

$$\sigma_{ni} = \sqrt{[(A(1)\sigma_1)^2 + (A(2)\sigma_2)^2 + \cdots + (A(n)\sigma_n)^2]} \tag{4}$$

Here $A(n)$ is the value of the apodization function for a given increment n. Again, if the standard deviation of the noise is equivalent for all points this equation can be rewritten as:

$$\sigma_{ni} = \sigma_s\sqrt{\sum_{n=1}^{ni} A(n)^2} \tag{5}$$

If all parameters other than the number of increments are constant then the relative change in the standard deviation of the noise is represented as a ratio of the two apodization functions:

$$\Delta\sigma_{ni} = \left[\frac{\sum_{m=1}^{ni_m} A(m)^2}{\sum_{n=1}^{ni_n} A(n)^2}\right]^{\frac{1}{2}} \tag{6}$$

Here ni_m is the revised number of increments while ni_n is the original number of increments. In the case of a 2D indirect plane of a 3D data set this treatment is directly extended using a double summation over the entire matrix of increments from both dimensions. For a 2D experiment the standard deviation of the noise may be written as:

$$\sigma_{ni\times ni_2} = \sigma_s\sqrt{\sum_{m=1}^{ni_2}\sum_{n=1}^{ni}(A_2(m)A_1(n))^2} \tag{7}$$

This expression can then be used to generate an equation for a radial sampled experiment. Radial sampling increments a single time delay and accordingly a single summation is included. However, as both apodization functions are still required, we have:

$$\sigma_{ni^{rad}} = \sigma_s\sqrt{\sum_{n=1}^{ni^{rad}}(A_2(n)A_1(n))^2} \tag{8}$$

Here both apodization functions are written here for clarity though in many cases a single equation suffices because of the common increment.

To evaluate the change in noise when converting from Cartesian sampling to radial sampling the ratio of Eqs. (7) and (8) is used.

$$\Delta\sigma_{ni} = \frac{\sigma_{ni^{rad}}}{\sigma_{ni\times ni_2}} \tag{9}$$

As a result of employing radial sampling the standard deviation of the noise is reduced. For example, if 64 points were collected in both indirect dimensions of a Cartesian sampled experiment compared to an equivalent resolution radial sampled experiment with 64 points in an angle plane the expected noise per angle will be reduced approximately 6.5-fold, although, as we will show below, the signal intensity is reduced simultaneously. Here a cosine-squared apodization function was used for both dimensions and a 45-degree radial sampling angle employed in the case of radial sampling.

The other relevant acquisition parameter that affects the standard deviation of the noise is the number of transient scans summed. Similar to the dependence of the noise on the number increments sampled, the change in the standard deviation of the noise as a function of the number of transients summed also obeys the variance sum law. The change in the standard deviation of the noise is commonly thought of as increasing by the square root of two as the number of transients is doubled. Using this fact, a continuous function for changing the number of transients is written as:

$$\Delta\sigma_{nt} = \sigma_s\sqrt{2^{\log_2(\frac{n_j}{n_i})}} \tag{10}$$

where σ_s is the standard deviation of the noise for a single transient scan, n_i is the original number of transient scans and n_j is the updated number of scans.

A final point regarding the noise that must be considered is the effect of the lower value comparison [10] when multiple angles are collected independently, processed and compared on an element basis. The lower value comparison is a popular treatment to remove artifact ridges when generating a final spectrum. Here we provide the relevant theory of how the standard deviation of the noise changes as a function of the number of angle spectra compared. For this analysis only regions of a spectrum that contain

noise are initially considered. The effects of peaks and ridges are considered subsequently.

In general, the lower value algorithm compares equivalent points from independent spectra and retains the lowest magnitude value to generate a final spectrum [10]. Previously, it has been assumed that the average deviation of the noise in the final spectrum decreases linearly as a function of the number of angles compared [14]. However, this description is insufficient to provide a means to analyze the change in the standard deviation of the noise as a result of lower value comparisons. To understand how the standard deviation of the noise decreases as a function of the number of angle spectra compared we start with a normal distribution of noise, Eq. (1). The lower value algorithm compares the magnitude of values. To analyze the distribution we use an absolute value of the normal distribution. The resulting probability density after reflecting all of the negative values upon zero results in twice the probability for a given value of x. The new distribution, substituting $y = |x|$ is written as:

$$p(y) = \frac{1}{\sigma}\sqrt{\frac{2}{\pi}}e^{-\frac{y^2}{2\sigma^2}} \tag{11}$$

Integrating the probability density function results in the cumulative distribution:

$$P(y \leqslant Y) = erf\left(\frac{y}{\sigma\sqrt{2}}\right) \tag{12}$$

Here the expression is simplified using the error function.

To determine how the standard deviation changes we need to determine how the probability for a single value of $y \leqslant Y$ varies after n trials. Noting that the probability for a single value that satisfies $y \leqslant Y$ is the complement probability that the same value satisfies $y \geqslant Y$ we have:

$$P^{\alpha}(y \geqslant Y) = 1 - P^{\alpha}(y \leqslant Y) \tag{13}$$

P^{α} is the cumulative probability for a single angle spectrum noise. Then the probability after n trials is the joint probability of each trial. Assuming that the noise is constant across the various sampling angles, the probability that all values y are greater than or equal to Y across the n radial sampling angles is:

$$P^{LV}(y \geqslant Y) = [1 - P^{\alpha}(y \leqslant Y)]^n \tag{14}$$

If the noise is not constant across all of the angle planes, such as in the case that a variable number of increments were collected per sampling angle, then Eq. (14) would be modified as the product of the individual cumulative probabilities. Continuing with assumption that the noise is constant across all sampling angles, the complement of Eq. (14), i.e. the probability that a value approaches zero, is then:

$$P^{LV}(y \leqslant Y) = 1 - \left(1 - erf\left[\frac{y}{\sigma\sqrt{2}}\right]\right)^n \tag{15}$$

where the cumulative probability has been substituted into the expression. The probability density is then the derivative of this expression, Eq. (16).

$$p^{LV}(y) = e^{-\frac{y^2}{2\sigma^2}} n\sqrt{\frac{2}{\pi}}\left(1 - erf\left[\frac{y}{\sigma\sqrt{2}}\right]\right)^{n-1} \tag{16}$$

Both the cumulative probability and the probability density are still in terms of the absolute value of x. To convert the cumulative probability into terms of x the function is partitioned equally between positive and negative components. When $x \geqslant 0$ the cumulative probability is divided by 2 and offset by one half to provide for equal distribution between positive and negative values. To determine the negative intensity probability the values for $x \geqslant 0$ are reflected upon zero and scaled appropriately. Thus the cumulative probability in terms of x is written as:

$$P^{LV}(x \leqslant X) = \frac{P^{LV}(y \leqslant Y)}{2} + .5, \quad x \geqslant 0 \tag{17a}$$

$$P^{LV}(x \leqslant X) = 1 - P^{LV}(|x|), \quad x < 0 \tag{17b}$$

The new probability distribution is shown in Fig. 1a as a function of number of angle spectra compared.

A similar procedure is followed to convert the probability density function into terms of x. In this case, when $x \geqslant 0$, the probability density function is divided by 2 and when $x < 0$ the probability density is the reflection of the positive values. The resulting probability density functions are:

$$p^{LV}(x) = \frac{p^{LV}(y)}{2}, \quad x \geqslant 0 \tag{18a}$$

$$p^{LV}(x) = p^{LV}(|x|), \quad x < 0 \tag{18b}$$

The probability density functions for a series of angle spectra are compared in Fig. 1b.

Finally, the change in standard deviation of the noise is determined by using the standard formula that relates the standard deviation to the probability density [13], shown in Eq. (19).

$$\sigma = \sqrt{\int_{-\infty}^{\infty} x^2 p^{LV}(x)dx} \tag{19}$$

The change in standard deviation is shown in Fig. 1c plotted as a function of the number of angle spectra compared. This figure demonstrates the substantial reduction in the standard deviation of the noise. For example, if 10 angles are compared the standard deviation of the noise is reduced 6.6-fold.

Above we have considered the effect of the lower value comparison with the assumption that no peaks or ridges were present in the noise distribution. The effect of the lower value comparison on peak intensity will be considered subsequently. In the case when a ridge is present in the lower value comparison, all of the values from the noise region of a non-ridge spectrum are retained as the ridge has an amplitude greater than the magnitude of the noise intensity. To determine the change in noise at this spectrum point, the same theory can be used, but excluding the ridge angle from the total count of number of angles.

The signal terms are now analyzed with respect to the number transients, increments and lower value comparison. The signal intensity at a single point of the two indirect dimensions (ω_i, ω_j) of a 3D Cartesian sampled NMR experiment is represented after apodization and Fourier transformation:

$$S^{Cart}(\omega_i, \omega_j) = n_t A \sum_{t_2}^{t_2^{max}} \sum_{t_1}^{t_1^{max}} \cos^2(\omega_i t_1) e^{-R_1 t_1} \cos^2(\pi t_1 / 2t_1^{max}) \times \cos^2(\omega_j t_2) e^{-R_2 t_2} \cos^2(\pi t_2 / 2t_2^{max}) \tag{20}$$

Here A is a scalar representing the analog–digital conversion, n_t is the number of transients and R is the combined transverse and longitudinal relaxation rates. For clarity only the cosine–cosine quadrature component is included.

The signal intensity is a sum of a random noise value and the mean signal described by Eq. (20). The distribution of noise will have effects when converting from Cartesian to radial sampling because the maximum signal plus the noise term is what is selected when calculating the signal-to-noise ratio. If we assume that the noise intensity is small in comparison to the peak intensity, we can initially exclude the noise when analyzing the change in signal upon converting from Cartesian to radial sampling. Therefore, only

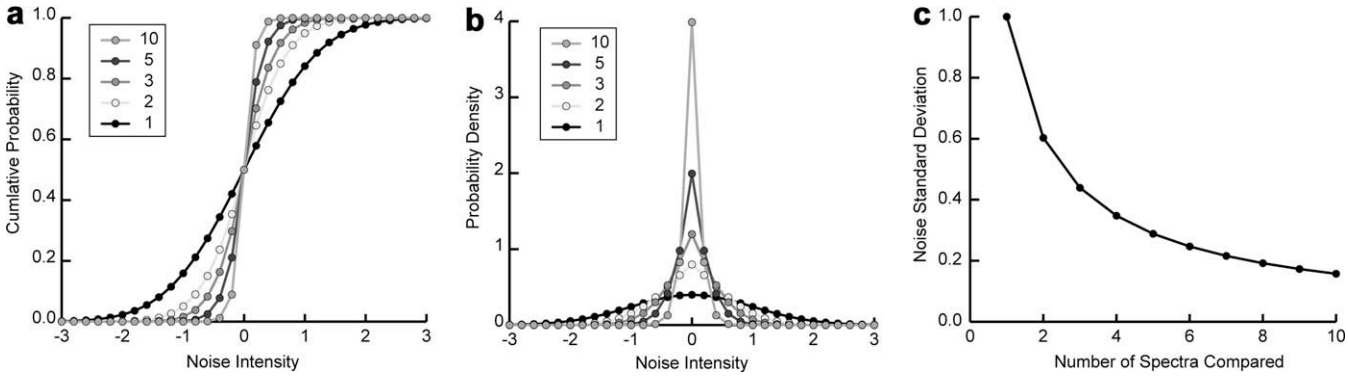

Fig. 1. The effect of the lower magnitude comparison on the noise is demonstrated as a function of number of angle spectra compared. The probability distribution function is shown in (a). The cumulative probability is plotted against the noise intensity for 1 (no comparison), 2, 3, 5 and 10 angle spectra comparisons. The corresponding probability density plots are shown in (b) for the same numbers of angle comparisons. The change in the standard deviation of the noise is plotted against the number of angle spectra compared in (c).

the change in mean signal is used. The noise term will be reintroduced when calculating the effects of the lower value comparison, when the change in signal is directly dependent upon the standard deviation of the noise.

In the case of radial sampling Eq. (20) is modified to account for a common increment τ, such that the equation for the maximum signal is written as:

$$S^{rad}(\omega_i,\omega_j) = n_t A \sum_{\tau}^{\tau^{max}} \cos^2(\omega_i \tau \cos(\alpha)) \cos^2(\omega_j \tau \sin(\alpha)) \times e^{-(R_1 \cos(\alpha)+R_2 \sin(\alpha))\tau} \cos^2(\pi\tau/2\tau^{max}) \quad (21)$$

Here the apodization functions have been reduced to a single function because a cosine-squared apodization is used for both dimensions, which leads to a double angle identity that combines the terms (see above). From Eqs. (20) and (21) it is apparent that increasing the number of transients linearly increases the signal. Increasing the number of increments also increases the signal but, in that case, the signal is scaled by the apodization and relaxation terms.

The change in maximum signal intensity when converting from Cartesian sampling to radial sampling is determined by taking the ratio of Eq. (20) to Eq. (21).

$$\Delta S = \frac{S^{cart}}{S^{rad}} \quad (22)$$

As a result of scaling the signal by apodization and relaxation when converting from Cartesian sampling to radial sampling the change in mean signal is not as significant as might be initially perceived. For example, if two experiments are collected, both requiring the same amount acquisition time, where the Cartesian sampled experiment uses 60 increments in both indirect dimensions and 4 transients and the radial sampled experiment used 60 increments, 10 angles and 24 transients, the expected reduction in signal per angle is approximately 5-fold compared to the 60-fold reduction in acquisition points.

The signal intensity is also modified by the lower value comparison as a result of the noise that influences the maximum signal. We now describe the change in the mean signal intensity and standard deviation of the signal intensity distribution to determine the effects of the lower value comparison. The approach to determine the change in the mean signal intensity is similar to the treatment used to determine the change in the noise distribution, but importantly, the distribution is not centered upon zero and therefore the mean of the distribution changes as a function of the number of angle spectra compared with the lower value comparison.

In the case of lower value comparison for a peak, the intensity distribution is offset from zero by the peak amplitude. Therefore, the lower value is selecting the smallest magnitude value in the distribution rather than the point closest to the mean of the distribution, as it would in the case of noise symmetric about zero. The lower value comparison selection moves the distribution towards zero resulting in a change in both the mean and standard deviation of the peak intensity distribution. To generally demonstrate the changes we will use a normal distribution that is centered upon zero and then select for the minimum value, rather than the minimum magnitude value. This allows one to easily determine the relative changes to both the standard deviation and mean, which can be extended to any peak intensity distribution.

As before, we start with a normal distribution with a probability density written as:

$$p(x) = \frac{1}{\sqrt{2\pi}} e^{-\frac{x^2}{2}} \quad (23)$$

Unlike the lower value description for the noise the absolute value is not employed. The density function is integrated to determine the cumulative distribution, Eq. (24).

$$P(x \leqslant X) = \frac{1}{2} + \frac{1}{2} erf\left(\frac{x}{\sqrt{2}}\right) \quad (24)$$

As before, utilizing the fact that the probability of a single value of $x \leqslant X$ is the complement of the probability that all of the values have a value $x \geqslant X$. The cumulative probability of the distribution after comparing n spectra is:

$$P(x \leqslant X) = 1 - \left(\frac{1}{2} - \frac{1}{2} erf\left(\frac{x}{\sqrt{2}}\right)\right)^n \quad (25)$$

The resulting change in the cumulative distribution as function of lower value comparisons is shown in Fig. 2a. Note that the mean of the distribution changes as the number of comparisons are increased. The new probability density is determined by solving the derivative of Eq. (25).

$$p(x) = \frac{1}{\sqrt{2\pi}} e^{-\frac{x^2}{2}} n\left(\frac{1}{2} - \frac{1}{2} erf\left(\frac{x}{\sqrt{2}}\right)\right)^{n-1} \quad (26)$$

The resulting probability densities are shown in Fig. 2b.

Finally, the change in the mean and standard deviation of the distribution can be determined using the standard equations, where the change in the mean of the distribution (μ) is determined as follows:

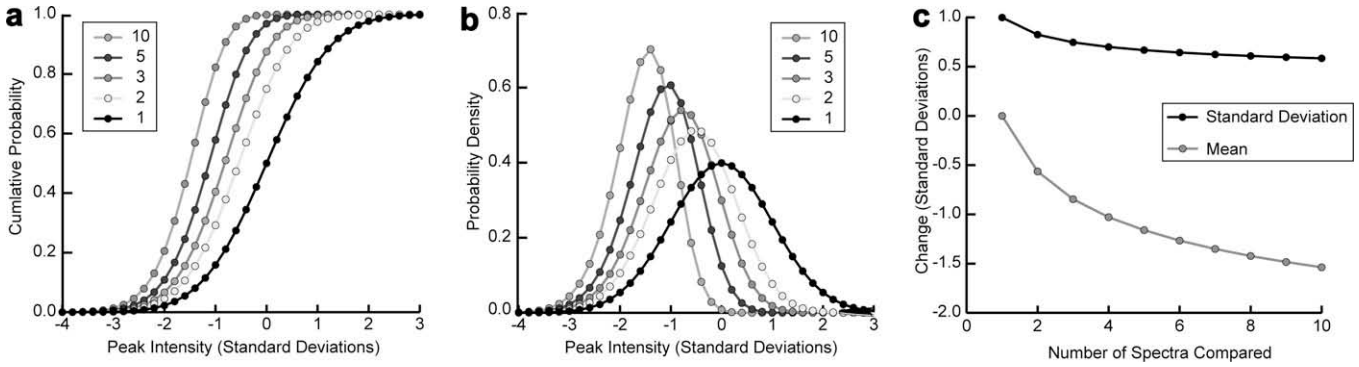

Fig. 2. The effect of the lower magnitude comparison on the distribution of signal intensity is demonstrated as a function of number of angle spectra compared. The probability distribution function is shown in (a). The cumulative probability is plotted against the peak intensity for 1 (no comparison), 2, 3, 5 and 10 angle spectra comparisons. The corresponding probability density plots are shown in (b) for the same numbers of angle comparisons. The change in the standard deviation and mean of the peak intensity is plotted against the number of angle spectra compared in (c).

$$\mu = \int xp(x)dx \tag{27}$$

Accordingly, the change in the standard deviation is determined in the same manner as for the noise distribution, with the exception that the values need to be corrected for the non-zero mean, Eq. (28).

$$\sigma = \sqrt{\int (x-\mu)^2 p(x)dx} \tag{28}$$

Fig. 2c shows the change in the mean and standard deviation of the signal intensity distribution as a function of number of angle spectra compared.

The change in the signal is dependent upon the random noise. In this respect, the average change of the maximum signal intensity is simply the change in the mean of the intensity distribution. For example, if 10 angle spectra were compared using the lower value algorithm the expected decrease in the signal intensity is 1.5 times the standard deviation of the single angle plane spectrum noise.

Importantly, it is also possible to predict the largest possible decrease in signal intensity. If the spectrum noise is described by a normal distribution, then 99.7% of the values are within 3 standard deviations from the mean. This produces a range of signal intensity that covers 6 standard deviations. If a single angle spectrum has a maximum signal intensity of the mean signal plus 3 standard deviations of the noise, while another single angle spectrum has the same mean peak intensity, but this time, minus 3 standard deviations of noise then the potential change in peak intensity from the lower value comparison is 6 standard deviations. This concept is illustrated by the probability density curves shown in Fig. 2b. The maximum intensity value of the no lower value comparison spectrum is 3 standard deviations greater than the mean. After lower value comparison of ten angles the new distribution results in a minimum intensity value that is 3 standard deviations less than the original distributions mean.

We have outlined all of the components that influence the signal-to-noise when converting from Cartesian to radial sampling. This analysis makes the assumption that the peak intensities are such that no value will be obscured by the baseline noise. If a peak intensity is insufficiently intense, such that it is obscured by the baseline noise, then the probability statements are no longer valid. A weak peak that changes sign as a result of the noise will behave according to the lower value noise statistics and approach zero. To prevent the removal of a peak during the lower value comparison the acquisition parameters need to be tested by collecting preliminary data such as a face (projection) or single angle of the experiment. Additionally, the treatment presented here assumes the S/N of all angle spectra are comparable and therefore using a single angle to assess the signal-to-noise of the final spectrum is valid. If the effects of relaxation cause the sensitivity to vary between angles then the angle with the minimum sensitivity should be used as a preliminary test for sufficient sensitivity. Additionally if peaks have an inherent dynamic range then a peak with the weakest intensity one desires to reliably measure should be used as an indicator of sensitivity.

The extreme case of signal reduction during the lower value comparison informs us that the largest reduction in signal is 6 standard deviations of the noise of a single angle. Therefore, if the signal-to-noise of the single angle test spectrum is at least 6, the peak will be retained. The expected minimum signal-to-noise of the final peak is then at least the test angle peak intensity minus 6 standard deviations of noise divided by the standard deviation of the noise after lower value comparison. To faithfully retain true peaks during lower value comparisons, single angle spectra with S/N greater than 6 should be compared.

The change in S/N after lower value comparison is illustrated in Fig. 3. Here the probability density functions are shown, one each for the signal and noise before and after 10 lower value comparisons. The two noise probability densities demonstrate how the

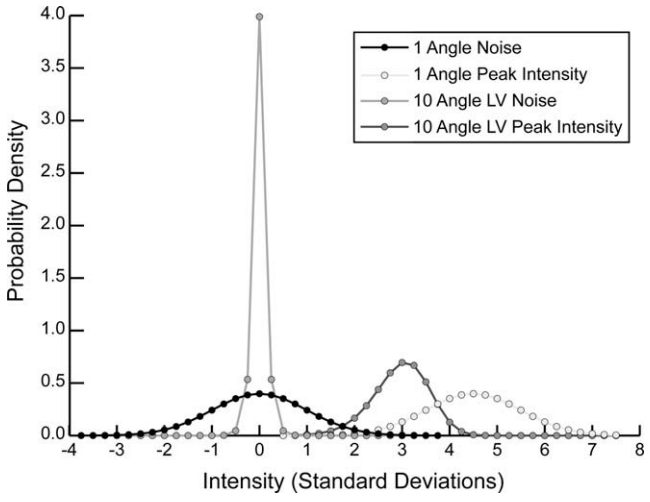

Fig. 3. A graphical representation of the probability density analysis to retain a peak and determine a target signal-to-noise ratio is shown. The distributions for both peak intensity and noise intensity before and after lower magnitude comparison are indicated. The lower magnitude probability densities were generated assuming the comparison of 10 angle spectra.

standard deviation of the noise decreases approximately 6.5-fold after 10 lower value comparisons. The signal intensity is also affected by the lower value comparison. Each of the angle spectra are collected independently and therefore will have uncorrelated noise causing the maximum intensity to be distributed as defined by the single angle peak intensity curve. After 10 lower value comparisons the distribution of intensities is shown. This curve has a mean intensity decrease of 1.5 times the standard deviation of the single angle noise.

The distributions defined in Fig. 3 also allow us to determine an expected signal-to-value for a set of radial sampling conditions and estimate the expected signal-to-noise change when converting from Cartesian to radial sampling. With the ability to determine how the noise and signal distributions change it is possible to define an expected signal-to-noise value. For example, if 10 radial sampling angles are collected we know the standard deviation of the noise will decrease by 6.5-fold and the maximum signal decrease is 6. Therefore, if a target signal-to-noise of 10 is desired the minimum signal needs to be at least 1.5 times the standard deviation of the noise and the test angle for a given set of acquisition parameters needs to have a signal-to-noise of at least 7.5. Using the same rationale it is possible to determine the change in signal-to-noise when converting from Cartesian to radial sampling. For a fixed experiment time and a required set of angles we are able to predict the change in the standard deviation of the noise using Eqs. (9), (10) and (19). Accordingly, we can also determine the change in the mean and standard deviation of the signal distribution using Eqs. (22), (27) and (28). The theoretical maximum gain is then estimated from Fig. 3. Note that this is the maximum gain because we are not accounting for the ridge values in the noise as discussed above.

The distributions and maximum signal reduction also allow for one to evaluate the feasibility of employing radial sampling in place of Cartesian sampling. We have recently presented an analysis on the number of sampling angles necessary to resolve a set of peaks. If the number of angles have been defined, the desired acquired digital resolution of each angle is determined and the total experiment acquisition time is fixed then it is possible to determine the maximum number of transients used in each experiment. If the number of transients is sufficient to meet the signal-to-noise criteria then radial sampling is feasible. If the required number of angles to resolve all peaks in a spectrum is not known this methodology also allows one to define the maximum number of angles that could be collected in a given experiment time in order to estimate the feasibility of application of radial sampling. Note that in the case where it is possible to collect a large number of angles that one should maintain some degree of spacing between angles to assure unique data from each angle. In this case it would be advisable to collect additional increments or transients.

Optimizing acquisition parameters to obtain a target single angle signal-to-noise while substantially reducing the noise with the lower value comparison is the essence of Sensitivity Enhanced *n*-Dimensional NMR (SEnD).

3. Results

The SEnD NMR strategy was tested with the HNCO experiment using a 20 μM ^{13}C,^{15}N-ubiquitin sample [15]. Three HxCO projections or faces of the HNCO, corresponding to a radial sampling angle of zero, were collected with 4, 8 or 16 transients (Fig. 4a–c). The corresponding full radial sampled three-dimensional experiments with ten angles equally distributed between 0 and 90 were collected to demonstrate the effects of varying *S*/*N* on the final lower magnitude spectrum. Representative two-dimensional slices of these spectra are shown in Fig. 4d–f. For this particular sample, use of four transients per free induction decay (FID) resulted in an average cross peak *S*/*N* of 3. This is well below the necessary *S*/*N* of 6 required by the SEnD approach and authentic peaks were indeed removed during lower value comparison (Fig. 4d). In the case of the spectrum obtained with eight transients the average *S*/*N* of peaks was 5.5. Since this is slightly below the SEnD criterion of 6 particular attention would need to be paid to the weakest peak(s). This is demonstrated in the Fig. 4e where the lower magnitude processed spectrum contains all of the peaks but the intensities and lineshapes are not uniformly accurate. When 16 transients are used all of the peaks have a signal-to-noise greater than the SEnD minimum of 6 and all are accurately represented in the lower value processed three-dimensional spectrum (Fig. 4f).

Statistical theory predicts that a significant sensitivity advantage over Cartesian sampling can be achieved for a fixed unit of acquisition time by applying the SEnD criteria to radial data acquisition providing that the minimum *S*/*N* criterion is met. This was tested by varying the number of transients while concomitantly changing the number of angles and keeping the total experiment time constant. The results are shown in Fig. 5. Here four radial angle experiments were collected on a 1 mM ^{13}C,^{15}N-ubiquitin sample, each requiring 7 h of data collection. A corresponding traditional Cartesian sampling spectrum was also obtained. The radial sampled experiments were collected with equivalent resolution to the Cartesian experiment but varied the number of transients and radial angles as follows: 32 transients with 5 angles, 16 transients with 9 angles, 8 transients with 18 angles, and 4 transients with 36 angles. Each radial sampled data set equally distributed the angles used between 0 and 90. A substantial *S*/*N* advantage is achieved over Cartesian sampling when a large number of angles are used. This advantage is achieved because of the reduction in noise from the lower value comparison. When a smaller number of angles are used the *S*/*N* is comparable to Cartesian sampling. This indicates that when only a small number of angles are available Cartesian sampling might be desirable.

To further illustrate the advantage of SEnD optimization, equivalent resolution HNCO spectra were collected on a 20 μM ubiquitin sample. When Cartesian sampling was used the total measurement time was 7 h and employed 4 transients and 36 complex increments in each of the indirect dimensions. For the SEnD optimization experiment, 5 angles, 32 transients and 36 quaternion data points were used for each angle. The requisite sensitivity of each angle spectrum was determined by collecting the HxCO face as a function of transients. The minimum number of transients required to satisfy the SEnD *S*/*N* criterion of 6 was determined to be 16, as demonstrated by Fig. 4c. Thirty-two transients were used to ensure that the SEnD criteria were met for all peaks in order to account for any variation in peak intensity as a function of sampling angle. This defines the total number of angles for the fixed total acquisition time to be 6, including 0 and 90 which require half of the quadrature components and therefore require half of the measurement time as compared to all other angles. The 6 angles were equally distributed between 0 and 90. Subsequent to generation of the final spectrum the spectrum was analyzed using the algorithms we have previously presented [11] and all peaks were determined to be resolved. Comparison of the conventional Cartesian spectrum and the SEnD optimized spectrum clearly indicates the distinct advantage that SEnD optimization offers (Fig. 6). Analysis of the SEnD optimized spectrum allowed all expected peaks to be identified and had *S*/*N* distributed between 13 and 25. The equivalent peaks in the Cartesian spectrum have a *S*/*N* distribution between 4 and 10, further demonstrating the advantage of SEnD optimization.

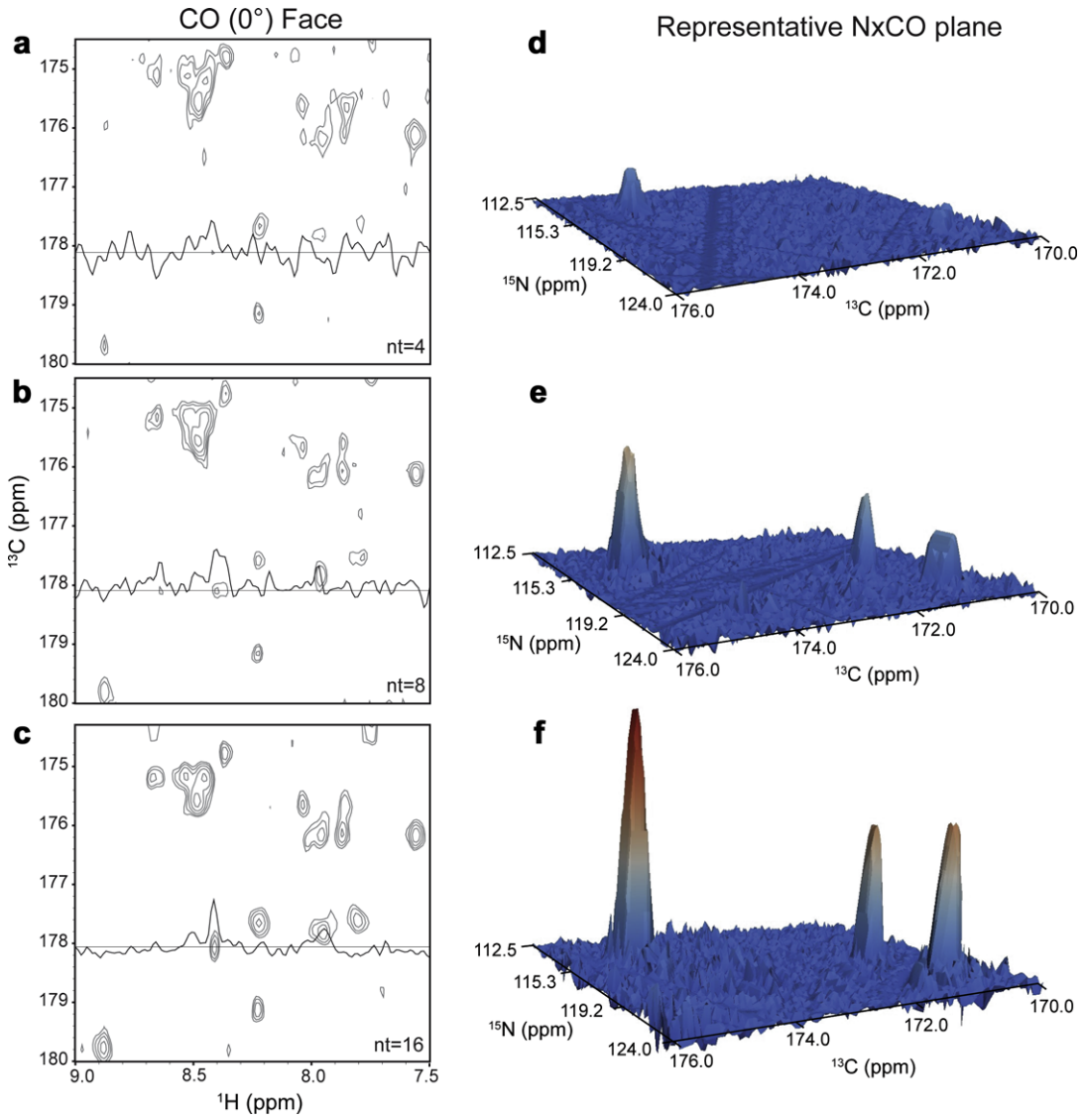

Fig. 4. The influence of signal-to-noise on peak retention during lower value comparison is demonstrated here using 20 μM ubiquitin. HxCO faces of the HNCO are used to assess the signal-to-noise of the radial sampled angle planes. The *S*/*N* was varied by changing the number of transients. 4, 8 and 16 transient spectra are shown in spectra a, b and c, respectively. One-dimensional slices are overlaid to illustrate the quality of the data. The average *S*/*N* of the three planes was 3 for 4 transients, 5.5 for 8 transients and 8.2 for 16 transients. Stacked plots of representative indirect planes of the lower magnitude spectra when 10 angles were compared are shown for each of the three settings of transients employed. The $n = 4$ transient/FID spectrum is shown in (d), 8 transient spectrum in (e) and 16 transient spectrum in (f).

4. Discussion

Previously, radial sampling has been utilized to optimize acquisition time and resolution, both without regard to sensitivity. Here we have defined the relevant criteria to determine the feasibility of utilizing radial sampling to boost both acquisition speed and resolution. Additionally, the defined criteria allow for simultaneous optimization of signal-to-noise. Various parameters are associated with the final sensitivity of a multidimensional NMR spectrum. Here we have demonstrated a method, employing radial sampling, to optimize the sensitivity of a multidimensional NMR experiment. This method exploits the redundancy of the data collection, providing that a minimum *S*/*N* is achieved in each component radial spectrum. This gives assurance that authentic peaks will survive application of the lower value algorithm. Generally, a minimum signal-to-noise of 6, for each angle spectrum as defined by the maximum signal reduction during lower value comparison, is sufficient. Effectively time allocated to increasing *S*/*N* in conventional experiments is redistributed to the collection of additional angle spectra that can be used to exponentially decrease the noise of the spectrum. Clearly the availability of cryogenically cooled probes and preamplifiers allows for the minimum *S*/*N* of individual angle spectra to more easily reached and emphasizes the synergy between high sensitivity probes and the SEnD methodology developed here. From a practical point of view, it is important to emphasize that it is possible to test for the satisfaction of the SEnD *S*/*N* criterion *prior* to acquisition of an entire data set. This is most easily accomplished by collecting a two-dimensional face of a three-dimensional experiment or the three-dimensional equivalent of a four-dimensional experiment. The projections allow one to conclude at the outset whether SEnD radial sampling is preferable to conventional Cartesian sampling with respect to final signal-to-noise.

The SEnD approach is generally applicable to all NH-based backbone resonance assignment experiments that are amenable to radial sampling. We have used a radial sampled (3,2)HNCO spectrum here to demonstrate the concepts, but the generality of the statistics allows for the extension of the methodology to four

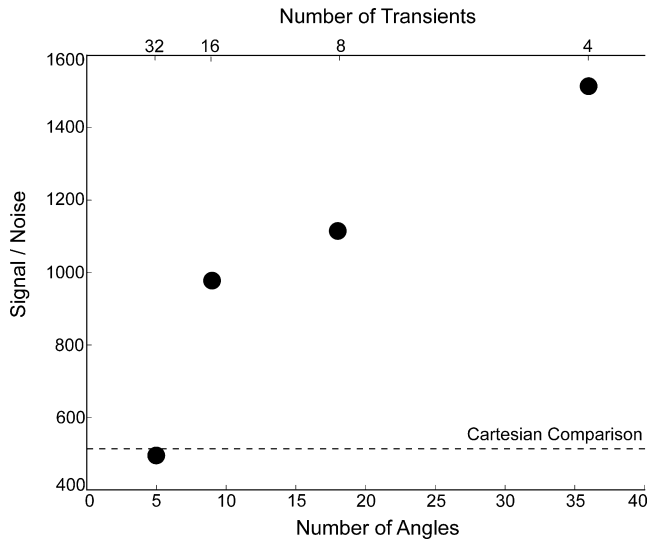

Fig. 5. The advantage of optimizing data collection parameters is shown here. Five experiments were collected on 1 mM ubiquitin, each requiring 7 h of measurement time. One experiment employed Cartesian sampling while the other four utilized radial sampling. The resolution was held constant by collecting 32 complex in both of the indirect dimensions of the Cartesian experiment, and 32 quaternion points for each angle in the radial sampled experiments. The four radial sampled experiments concomitantly varied the number of transients and angles to keep a constant experiment time. The four combinations used were 32 transients and 5 angles; 16 transients and 9 angles; 8 transients and 18 angles and 4 transients and 32 angles. The average *S*/*N* of all the peaks in the resulting lower magnitude spectra are plotted with the average *S*/*N* of the Cartesian experiment shown for reference.

dimensions, if not higher, as long as the SEnD criteria are satisfied. Such is the case for a (4,3) sampled experiment, where the criteria would be the same as the (3,2) sampled experiment presented here. Additionally, as we will report elsewhere, the sensitivity gain offered by the SEnD approach provides the opportunity for higher sensitivity and better digital resolution four-dimensional NOESY spectra to be obtained. The application of the SEnD approach in the context of quantitative or even semi-quantitative analysis of NOE peak intensities will require special consideration. This is because the largest negative deviation from a peaks mean is selected for during the lower magnitude comparison of all angle spectra. However, after application of the SEnD method to identify peaks, analyzing the individual angle spectra and treating them with the usual statistics for redundant measurement can potentially recover accurate intensities. Also, particular attention should be paid to the dynamic range of the peaks in this spectrum. Only peaks meeting the SEnD criteria will be enhanced in the final spectrum. Therefore careful attention is needed for the weakest peaks. This will be described in more detail elsewhere.

Finally, our objective here has not been to carry out a comparison of all of the sparse sampling and processing methods available. Rather we have focused on exploiting the redundancy of the data, unique to radial sampling, in a manner that substantially reduces the spectrum noise and aids in peak identification. It is possible to envision a similar approach that combines multiple random sampled spectra processed in combination with a lower value noise removal step. However, as a result of the distributed baseline artifacts associated with random sampling, the required number of transients needed to obtain the SEnD signal-to-noise criteria of 6 could prove to be prohibitive unless combined with an iterative "cleaning" method. Nevertheless, the SEnD criteria can be employed in conjunction with other methods capable of processing radial sampled data [10,12,16–19].

5. Methods

Recombinant ubiquitin was prepared as described [15]. NMR data was collected on either a 20 μM or 1 mM ^{13}C, ^{15}N uniformly labeled sample of human ubiquitin at 25 °C on a Bruker Avance III 500 MHz NMR spectrometer equipped with a 5 mm triple resonance TCI cryogenic probe. The sample was prepared in 50 mM potassium phosphate buffer pH 5.5 with 50 mM NaCl and 0.04% sodium azide in 90% H_2O/10% D_2O. NMR data was collected using a standard HNCO [20] or a modified version for radial sampling, such that $t_1 = t_1\cos(\alpha)$ and $t_2 = t_1(sw_1/sw_2)\sin(\alpha)$. The Cartesian experiment was collected using 36 complex points in both of the indirect dimensions for a total of 5184 FIDs. Each FID was the average of 4 transients and contained 512 complex points requiring approximately 7 h of measurement time. The spectral width was set to 12, 30 and 12 ppm for proton, nitrogen and carbon, respectively. The carriers for each dimension were set to 4.682, 114.93 and 174 ppm for proton, nitrogen and carbon, respectively. The maximum acquisition times for the nitrogen and carbon dimensions were 0.0237 and 0.0239 s, respectively. In the case of radial sampling all experimental parameters were set to equivalent values as the Cartesian experiment unless otherwise noted in the main text. All of the radial sampled experiments utilized 36 quaternion data points, requiring 4 quadrature components per data point expect for the 0 and 90 spectra which only require 2 quadrature components. In the case where 4 transients were used, each sampling angle plane required 12 min of measurement time. The angle spectra were processed independently using a direct 2D Fourier transform. Prior to Fourier transforming, the data was apodized with cosine-squared function to remove truncation artifacts and to approximate the correction for unequally spaced data [3]. The data was zero-filled to at least twice the number of incremented points. Following processing, individual angle spectra were compared using the lower value (magnitude) algorithm to remove the ridge artifacts [10]. The Cartesian sampled data was processed with corresponding apodization and zero filling. The fast Fourier transform was used in place of the direct 2D Fourier transform. All processing

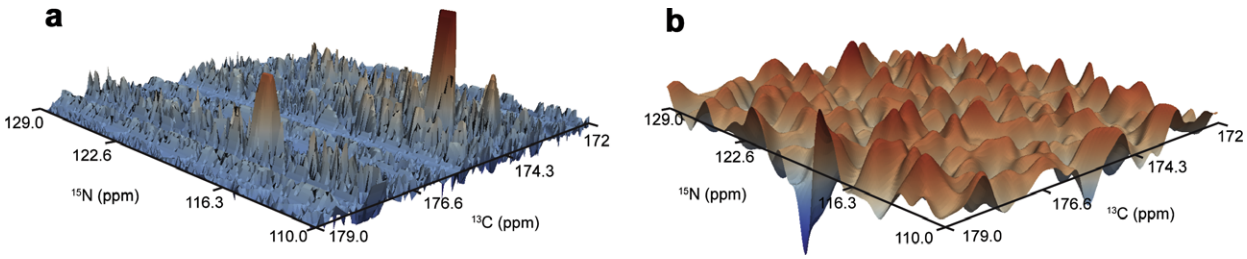

Fig. 6. Comparison of SEnD optimized radial sampling (a) and Cartesian sampling (b) of an HNCO spectrum obtained on a 20 μM ubiquitin. Both spectra required 7 h of acquisition time and were collected with equivalent resolution parameters. In the example shown, the SEnD spectrum has identifiable peaks while the corresponding peaks in the Cartesian spectrum are obscured by noise.

was done using an in-house program and visualized using Sparky [21].

Acknowledgments

This work was supported by a grant from the Mathers Foundation and an NSF MRSEC award (DMR-0520020). J.M.G. was an NIH pre-doctoral trainee during a portion of this work (GM 008275).

References

[1] B.E. Coggins, P. Zhou, Polar Fourier transforms of radially sampled NMR data, J. Magn. Reson. 182 (2006) 84–95.
[2] K. Kazimierczuk, W. Kozminski, I. Zhukov, Two-dimensional Fourier transform of arbitrarily sampled NMR data sets, J. Magn. Reson. 179 (2006) 323–328.
[3] D. Marion, Processing of ND NMR spectra sampled in polar coordinates: a simple Fourier transform instead of a reconstruction, J. Biomol. NMR 36 (2006) 45–54.
[4] B.E. Coggins, P. Zhou, Sampling of the NMR time domain along concentric rings, J. Magn. Reson. 184 (2007) 207–221.
[5] B.E. Coggins, P. Zhou, High resolution 4-D spectroscopy with sparse concentric shell sampling and FFT-CLEAN, J. Biomol. NMR 42 (2008) 225–239.
[6] K. Kazimierczuk, A. Zawadzka, W. Kozminski, Optimization of random time domain sampling in multidimensional NMR, J. Magn. Reson. 192 (2008) 123–130.
[7] K. Kazimierczuk, A. Zawadzka, W. Kozminski, I. Zhukov, Random sampling of evolution time space and Fourier transform processing, J. Biomol. NMR 36 (2006) 157–168.
[8] N. Pannetier, K. Houben, L. Blanchard, D. Marion, Optimized 3D-NMR sampling for resonance assignment of partially unfolded proteins, J. Magn. Reson. 186 (2007) 142–149.
[9] K. Kazimierczuk, A. Zawadzka, W. Kozminski, I. Zhukov, Lineshapes and artifacts in multidimensional Fourier transform of arbitrary sampled NMR data sets, J. Magn. Reson. 188 (2007) 344–356.
[10] E. Kupce, R. Freeman, Projection–reconstruction technique for speeding up multidimensional NMR spectroscopy, J. Am. Chem. Soc. 126 (2004) 6429–6440.
[11] J.M. Gledhill, A.J. Wand, Optimized angle selection for radial sampled NMR experiments, J. Magn. Reson. 195 (2008) 169–178.
[12] J.M. Gledhill Jr., B.T. Walters, A.J. Wand, AMORE-HX: a multidimensional optimization of radial enhanced NMR-sampled hydrogen exchange, J. Biomol. NMR 45 (2009) 233–239.
[13] G.P. Wadsworth, J.G. Bryan, Introduction to Probability and Random Variables, McGraw-Hill, New York, 1960.
[14] R.A. Venters, B.E. Coggins, D. Kojetin, J. Cavanagh, P. Zhou, (4,2)D Projection–reconstruction experiments for protein backbone assignment: application to human carbonic anhydrase II and calbindin D (28 K), J. Am. Chem. Soc. 127 (2005) 8785–8795.
[15] A.J. Wand, J.L. Urbauer, R.P. McEvoy, R.J. Bieber, Internal dynamics of human ubiquitin revealed by ^{13}C-relaxation studies of randomly fractionally labeled protein, Biochemistry 35 (1996) 6116–6125.
[16] H.R. Eghbalnia, A. Bahrami, M. Tonelli, K. Hallenga, J.L. Markley, High-resolution iterative frequency identification for NMR as a general strategy for multidimensional data collection, J. Am. Chem. Soc. 127 (2005) 12528–12536.
[17] S. Hiller, F. Fiorito, K. Wuthrich, G. Wider, Automated projection spectroscopy (APSY), Proc. Natl. Acad. Sci. USA 102 (2005) 10876–10881.
[18] D. Malmodin, M. Billeter, Multiway decomposition of NMR spectra with coupled evolution periods, J. Am. Chem. Soc. 127 (2005) 13486–13487.
[19] J.W. Yoon, S. Godsill, E. Kupce, R. Freeman, Deterministic and statistical methods for reconstructing multidimensional NMR spectra, Magn. Reson. Chem. 44 (2006) 197–209.
[20] D.R. Muhandiram, L.E. Kay, Gradient-enhanced triple-resonance 3-dimensional NMR experiments with improved sensitivity, J. Magn. Reson. Ser. B 103 (1994) 203–216.
[21] T.D. Goddard, D.G. Kneller, SPARKY 3, University of California, San Francisco.